CHAPTER 4

TEST RESULTS AND ANALYSIS OF TEST RESULTS

Load-Deflection Relationship

As shown in Fig. 4.1, the responses at mid-span deflections under load of B1 and B2 are about the same. At first stage of loading, the deflections were proportional to the loading, the deflections were proportional to the loads and behaved elasticly until the tensile cracks at bottom fiber in the zone of maximum moment were formed at the loads of about 830 kg. for B1 and 960 kg. for B2. The neutral axes were suddenly shifted toward the compression face as shown in Fig. 4.7 and 4.8. At further stages of loading, more cracks were formed and the previous ones were propagated toward the neutral axes. The first visible crack in shear span was observed at the load of 1390 kg. for B1 and 2150 kg. for B2, then the neutral axes began to stabilize and other portion of elastic behavior was observed. This stage ended at the loads of about 7100 kg. for B1 and 6000 kg. for B2. It should be noted that the deflections increased more rapidly while the loads were nearly constant and the neutral axes shifted very slightly before failure.

For B3, its flexural rigidity was less than that of B1 or B2 with more deflections at the same load levels. The first major loss of stiffness occured at the load at 830 kg. when the vertical flexural cracks occured in the region of maximum moment. The neutral axis suddenly shifted toward the compression face as shown in Fig. 4.9. At further stages of loading, more cracks were formed but they were less

than those at B1 and B2. The cracks in shear spans and the neutral axis moved further than those ones at B1 and B2. Its elastic behavior was ended at the load of 4840 kg. This point was the start at a tension failure behavior. It was initiated by inelastic deformation of the tensile reinforcement. The additional increase in load carrying capacity as noticed in Fig. 4.1 was a result of large additional steel strains which caused large angle changes and deflections due to onset of strain hardening and the length of the internal lever arm.

Load-deflection curves of B4 and B5 shown in Fig. 4.1 are rather different from those ones stated above. After their first losses of flexural rigidity at the load of 600 kg. for B4 and 590 kg. for B5, the neutral axes moved forward rapidly and then began to stabilize until failure as shown in Fig. 4.10 for B4 and Fig. 4.11 for B5. It is is not obviously shown the ends of their elastic behavior. The amounts of cracks of B4 and B5 were much less than those of B1, B2 and B3 but the crack widths were bigger. The ultimate loads of B4 and B5 were 2880 and 2000 kg. respectively. For B5, the longitudinal reinforcements were pulled apart. Strain hardening in both beams could not be observed.

Fig. 4.2 to Fig. 4.6 respresent load-deflection responses of B1 to B5, each beam represented with six curves. The first curve, abbreviated as Obs., was obtained from the test results. The second one, abbreviated as I_{inst} its mid-span deflections were obtained by using observed strain distributions to find instantaneous moment of inertia of the sections and then substituting them with corresponding applied loads, span length and modulus of elasticity into equation (2.27). The third one, abbreviated as I_{eff}, its mid-span deflections were obtained by

substituting effective moment of inertia, in equation (2.16), with corresponding applied loads and other values into equation (2.25). The fourth one, abbreviated as Para, its mid-span deflections were obtained by assuming parabolic shape in concrete compressive stress distribution conforming to internal force equilibrium and strain compatibility to find internal resisting moment and instantaneous moment of inertia then transform internal resisting moment to equivalent applied loads, after that substitute them with other values into equation (2.27). The fifth one abbreviated as Tri, its mid-span deflections were obtained in the same way as those in Para except that concrete compressive stress distribution was assumed in triangular shape. The last one, abbreviated as Straight, its mid-span deflections were obtained by substituting moments of inertia of uncracked and cracked sections, shown in equation (2.2) and (2.6) respectively, with corresponding applied loads and other values into equation (2.24). The mid-span deflections of Para and Tri were plotted against equivalent applied loads while the others applied loads and samples of calculation shown in Appendix.

As shown in Fig. 4.2 to Fig. 4.6, it should be noted that test beams with low longitudinal reinforcements of which the value of reinforcement index, ω, varied from 0.041 for B5 to 0.061 for B4, indicated good agreement of mid-span deflection responses both before and after crack predicted by working stress method. The beams with larger reinforcements of which the value of reinforcement index, w, varied from 0.092 for B3 to 0.121 for B1 indicated good agreement of those ones by suing parabolic or triangular shape in compressive stress distribution with strain compatibility to find equivalent external forces and instantaneous moment of inertia then substituting them into equation

(2.27), or by substituting effective moment of inertia, in equation (2.16) into equation (2.25) and effective moment of inertia were conformed to instantaneous moment of inertia obtained from strain measurements during the tests only for test beams of which the value of reinforcement index varied from 0.041 to 0.092.

It should be noted from Table 4.1 shown the ratios between applied load corresponding to limitted mid-span deflection $\ell/180$[1] and ultimated load of each test beam that the maximum load of the beam could be as high as 44 % of the ultimate load as the maximum mid-span deflection controlled by $\ell/180$.

Fig. 4.12 shows the relationship between reinforcement index, w, and maximum observed reinforcement strain at failure. This assures that yield strengths were obtained in longitudinal reinforcements of all test beams since yield strain of those ones was 0.008. The relationship may be expressed by empirical formula as:

$$\varepsilon = 0.0317-0.150\ \omega \qquad \text{.....(4.1)}$$

However the range of reinforcement index is between 0.041 and 0.121.

Fig. 4.13 shows the maximum compressive strain plotted against the corresponding concrete strengths of all test beams compared with the result of Pochanart[13] and Nedderman[10]. It can be seen that maximum compressive strain in this study varies from 0.0022 to 0.0037 and the average is 0.0027. It is slightly less than that indicated in 1977 ACI Code.

Ductility

As stated before that the ductility index may be defined as the ratio of ultimate to yield curvature and it should be 455 to 5.7 for ordinary reinforced concrete members as suggested by Furlong[16]. In this study the ratio between span length to depth was 11.7 then substituting it into equation (2.20) yielded that the ductility index should be 3.7. It can be seen in Fig. 4.19 that the ultimate curvatures can not be obtained directly by measurement method as stated in Chapter 3. However, the ductility index could be approximately obtained from the ratio of ultimate to yield deflection at corresponding position. The ductility indexes of all test beams are tabulated in Table 4.1. The index ranges from 1.73 to 2.91 and the average is about 2.26. One should be noted that the higher the reinforcement index, the lower the ductility index.

Fig. 4.19 shows the responses of mid-span curvature under loaded, in term of moment, of all test beams, resulted from observed strain distributions shown in Fig. 4.14 to Fig. 4.18 for B1 to B5 respectively. The curves resemble the load-deflection curves presented in Fig. 4.1. The curves are linear in the initial stages. With an increase in moment, the flexural rigidities of the test beams were reduced. The reduction was greater for the lightly reinforced beams, B4 and B5, than for the more heavily reinforced ones, B1, B2 and B3.

Flexural Strength

All test beams were failed in flexure mode of tension failure in the maximum moment region thus represented the maximum

loads the beams could resist. The maximum load capacity of each beam obtained by different approaches was compared to the observed test results as shown in Table 4.2.

By using compressive stress distribution as proposed by Nedderman yielded the strength ratio of calculated moment to observed one was ranged from 0.919 to 1.219 and the average was 1.045 with a standard deviation of 11.390 %.

For triangular stress distribution, the average strength ratio varied from 0.916 to 1.216 and the average was 1.042 with a standard deviation of 11.406 %.

By using ACI (318-77) equivalent rectangular stress distribution the strength ratio varied from 0.833 to 1.024 and the average was 0.944 with a standard deviation of 10.154 %.

Crack Pattern and Mode of Failure

Since very-high strength concrete is relatively weak in tension and strong in compression cracks will form the first in regions of tensile stress which exceeds its tensile strength. The longitudinal reinforcement does not prevent cracking even though it may tend to distribute cracks along the beam. The location, size and shape of cracks would indicate the zone of maximum tensile stress.

Two types of cracks were encountered in the tests: flexural and diagonal tension cracks. Flexural cracks result from tensile stresses caused by bending moment while diagonal tension cracks results from the inclined tensile stresses in a region of combined bending moment and shear.

In all test beams, the first cracks were flexural cracks in the constant moment region. They started at the bottom of the beam and propagated vertically. Further loading would cause flexural cracks in the shear spans. Such cracks were inititated by tensile stress at the bottom fiber as vertical cracks and tended to bend toward the loaded point in the regions of combined shear and bending moment.

Crack patterns for all test beams are shown in Fig. 4.20 to 4.24. For B1, B2 and B3, of which the reinforcement indexes varied from 0.092 to 0.121. Flexural cracks appeared first in the portion of maximum moment at about 11, 14 and 16 % of the ultimate loads for B1, B2 and B3 respectively. The cracks propagated higher as the loads were increased. A few flexural cracks also appeared in the shear span regions and crack spacing was about 7-14 cm. apart. At further stages flexural-shear cracks occured at about 65 % of the ultimate loads. At failure the beams were collapse suddenly and explosively and some portions of concrete on the compression face were spalled apart. It generally occured in the maximum moment zone and depth of the spalled concrete could be as far as the location of neutral axis.

For B4 and B5 the reinforcement indexes were 0.061 and 0.041. The flexural first cracks occured at about 20 and 30 % of the ultimate loads for B4 and B5 respectively in the portion of constant bending moment. Flexural-shear cracks in shear span regions of B4 and B5 were less than those of B1, B2 and B3 in the same regions due to the lower load capacity. The failure of B4 was sudden and explosive but the one of B5 was gentle because its reinforcements were pulled apart.

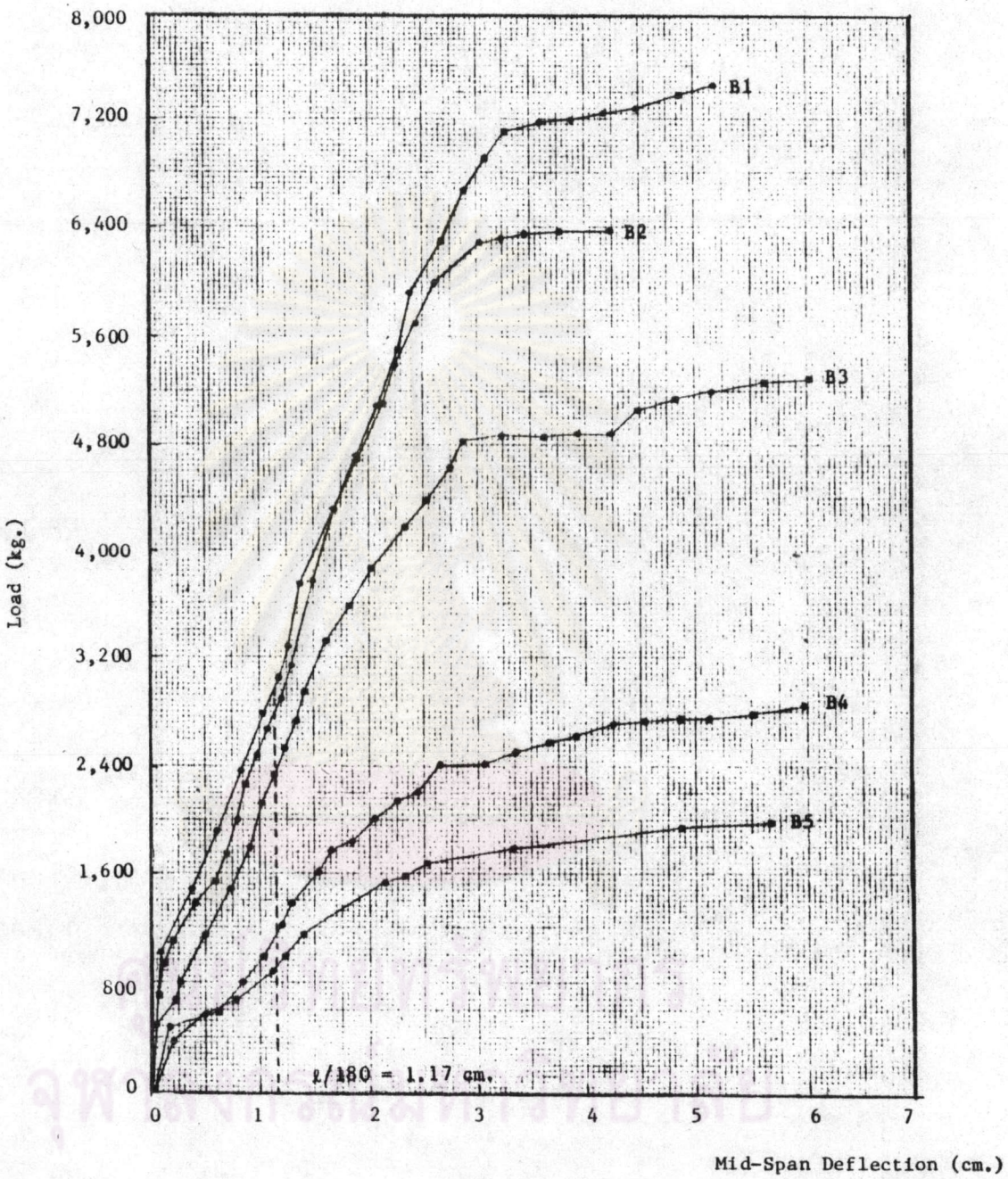

Fig. 4.1 Load-Deflection Responses of Test Beams

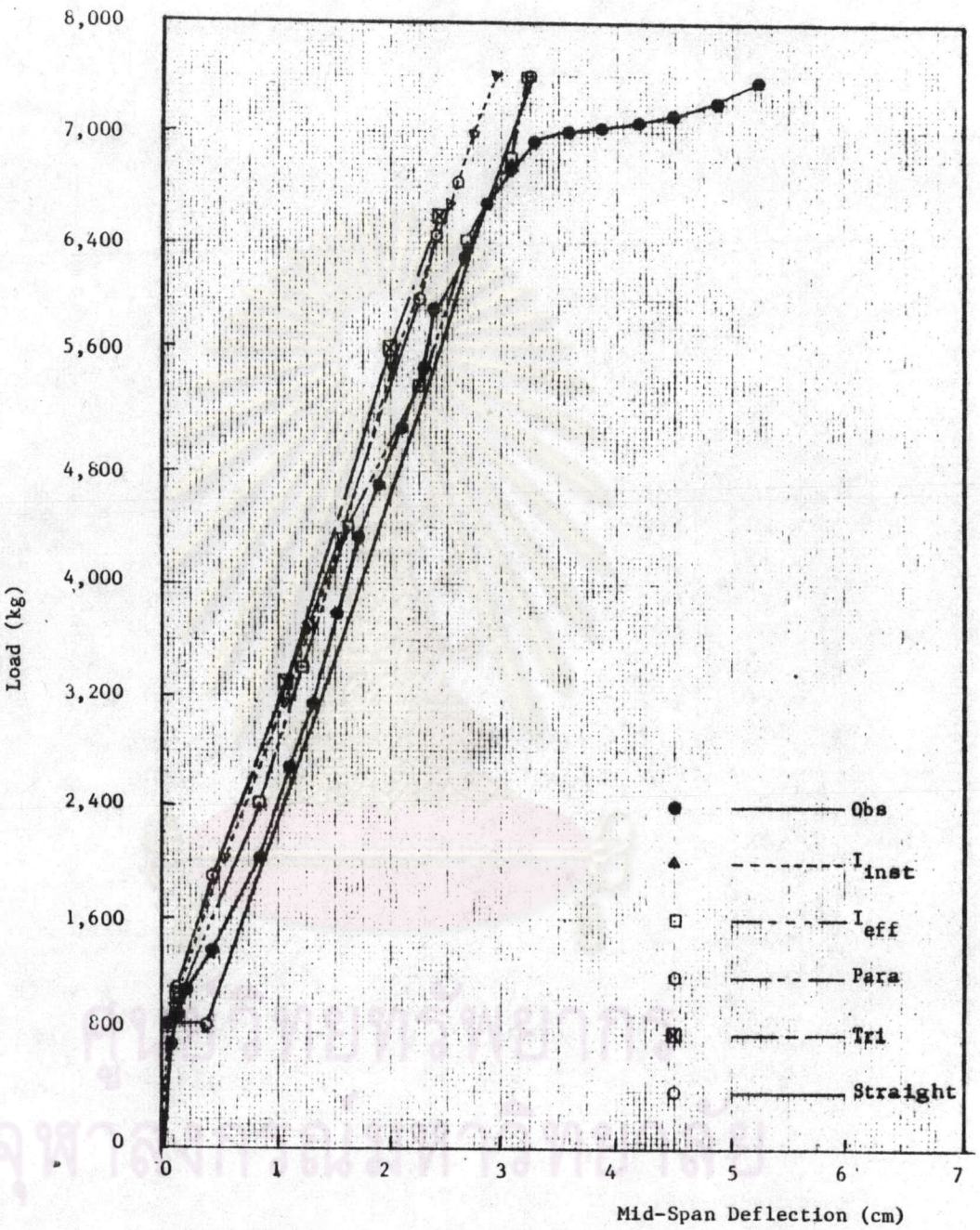

Fig. 4.2 Observed and Calculated Load-Deflection Curve of B1

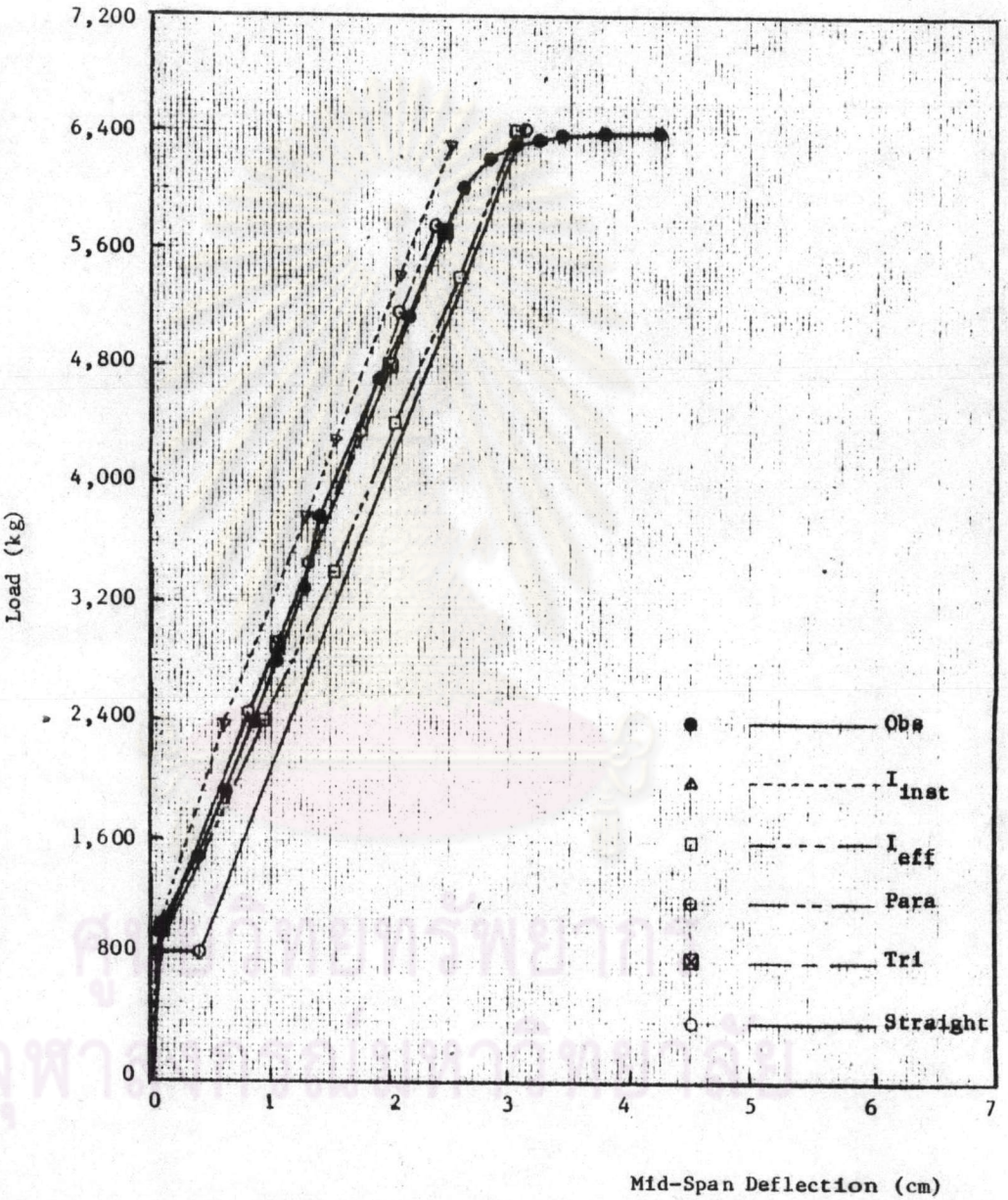

Fig. 4.3 Observed and Calculated Load-Deflection Curve of B2

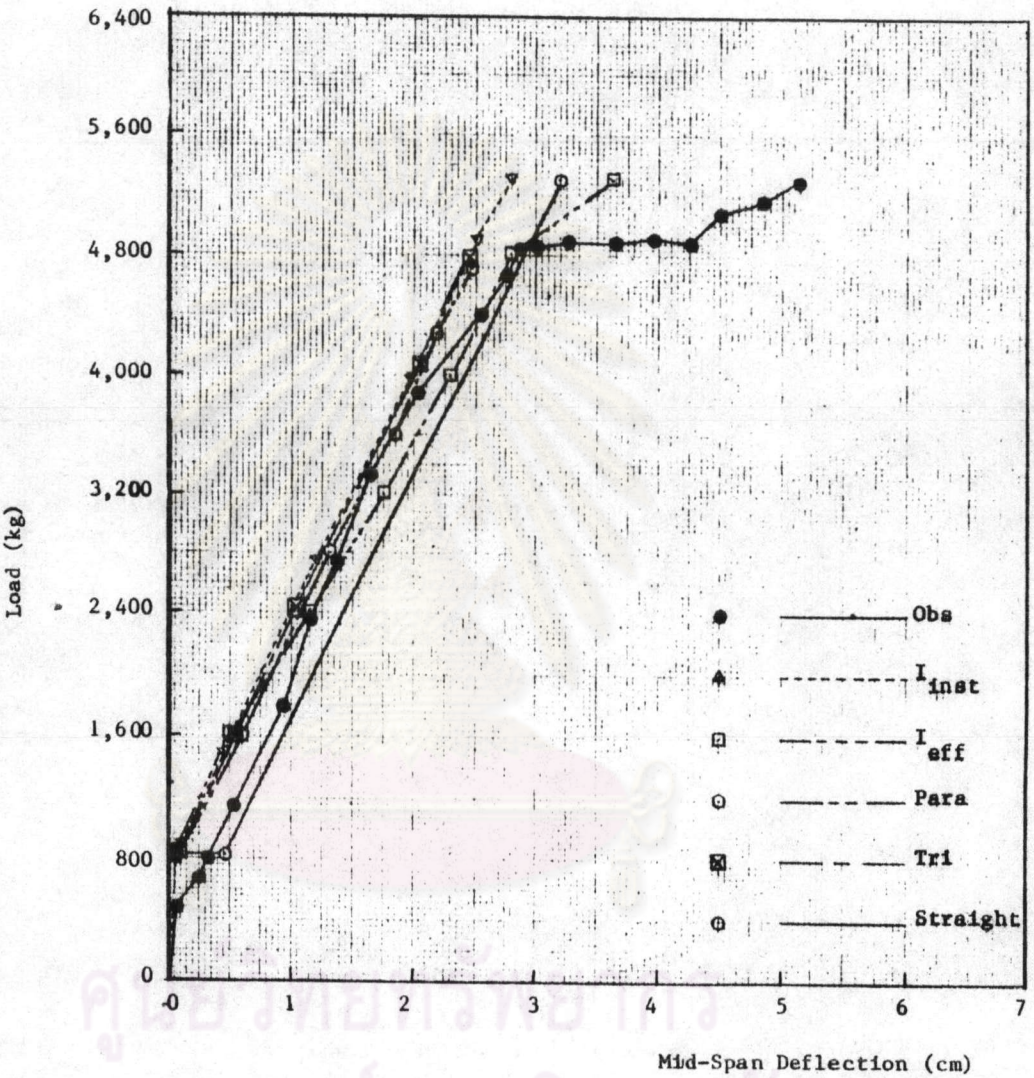

Fig. 4.4 Observed and Calculated Load-Deflection Curve of B3

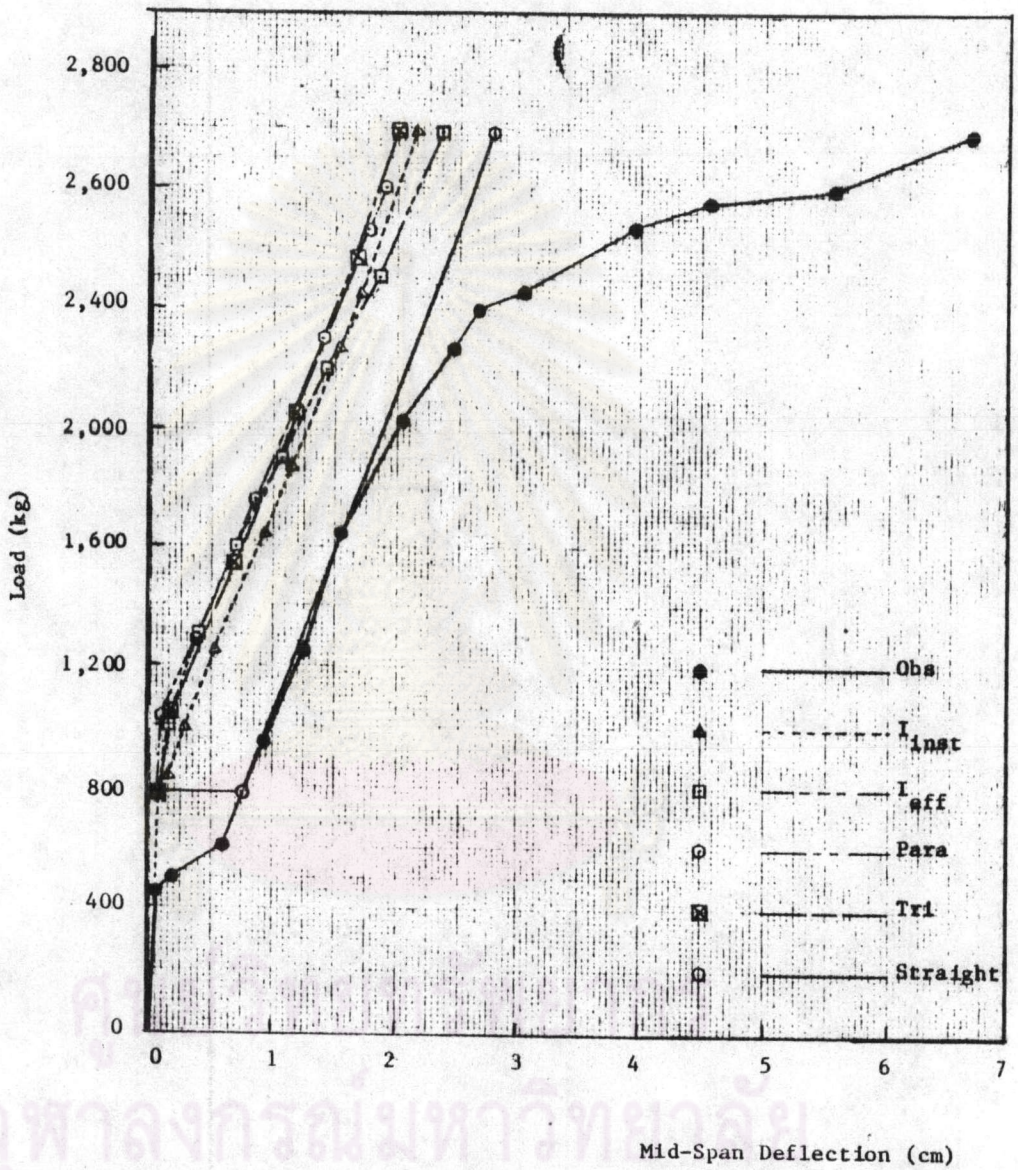

Fig. 4.5 Observed and Calculated Load-Deflection Curveof B4

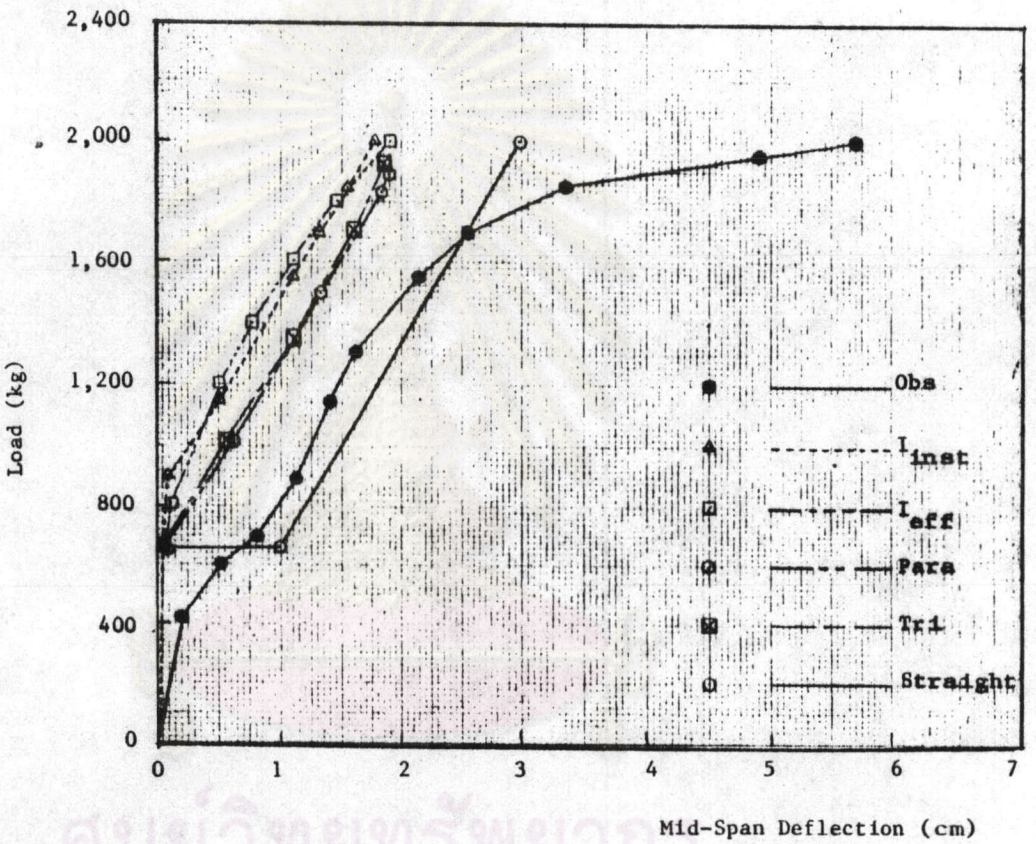

Fig. 4.6 Observed and Calculated Load-Deflection Curve of B5

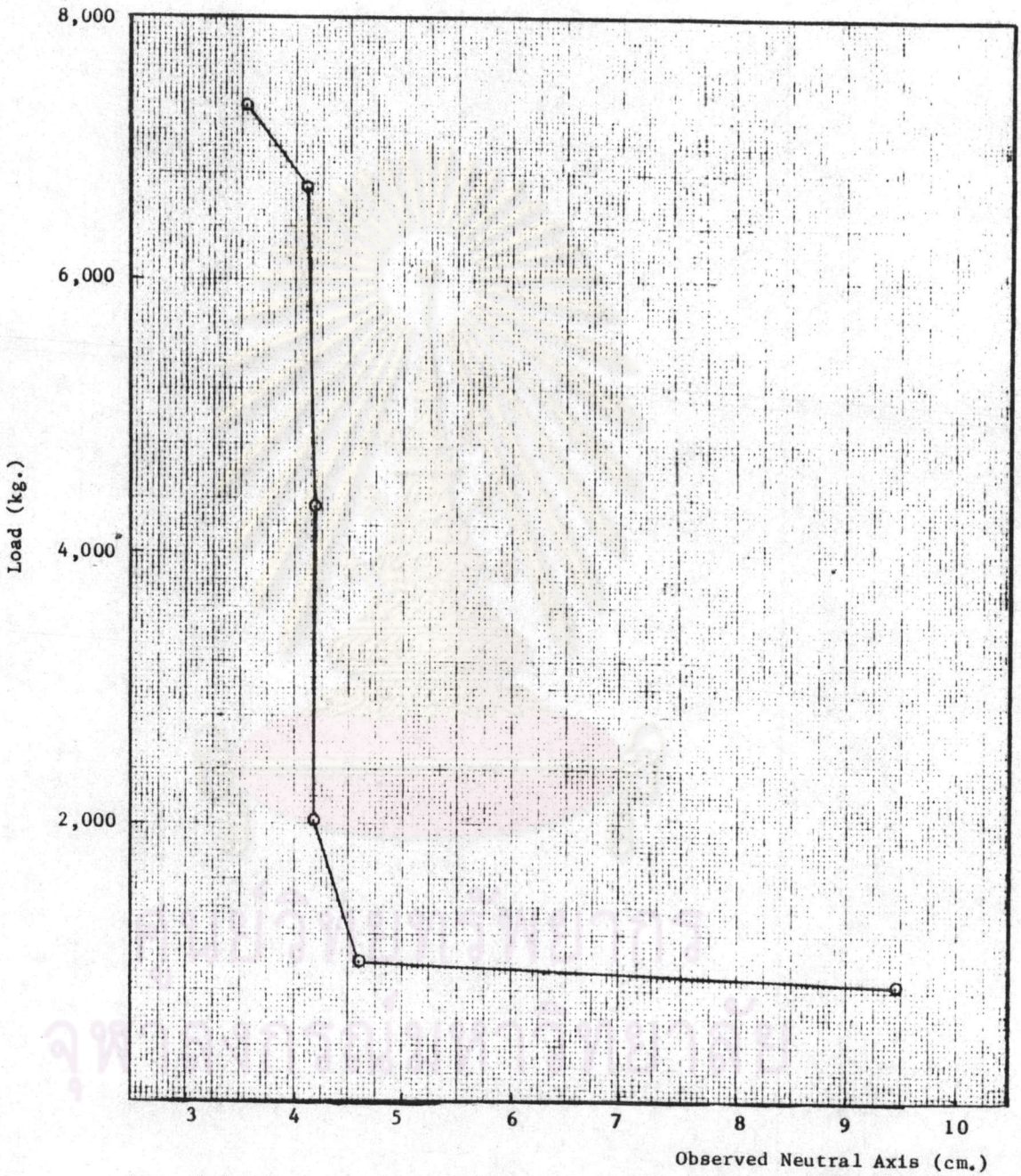

Fig. 4.7 Relationship Between Load and Observed Neutral Axis of B1

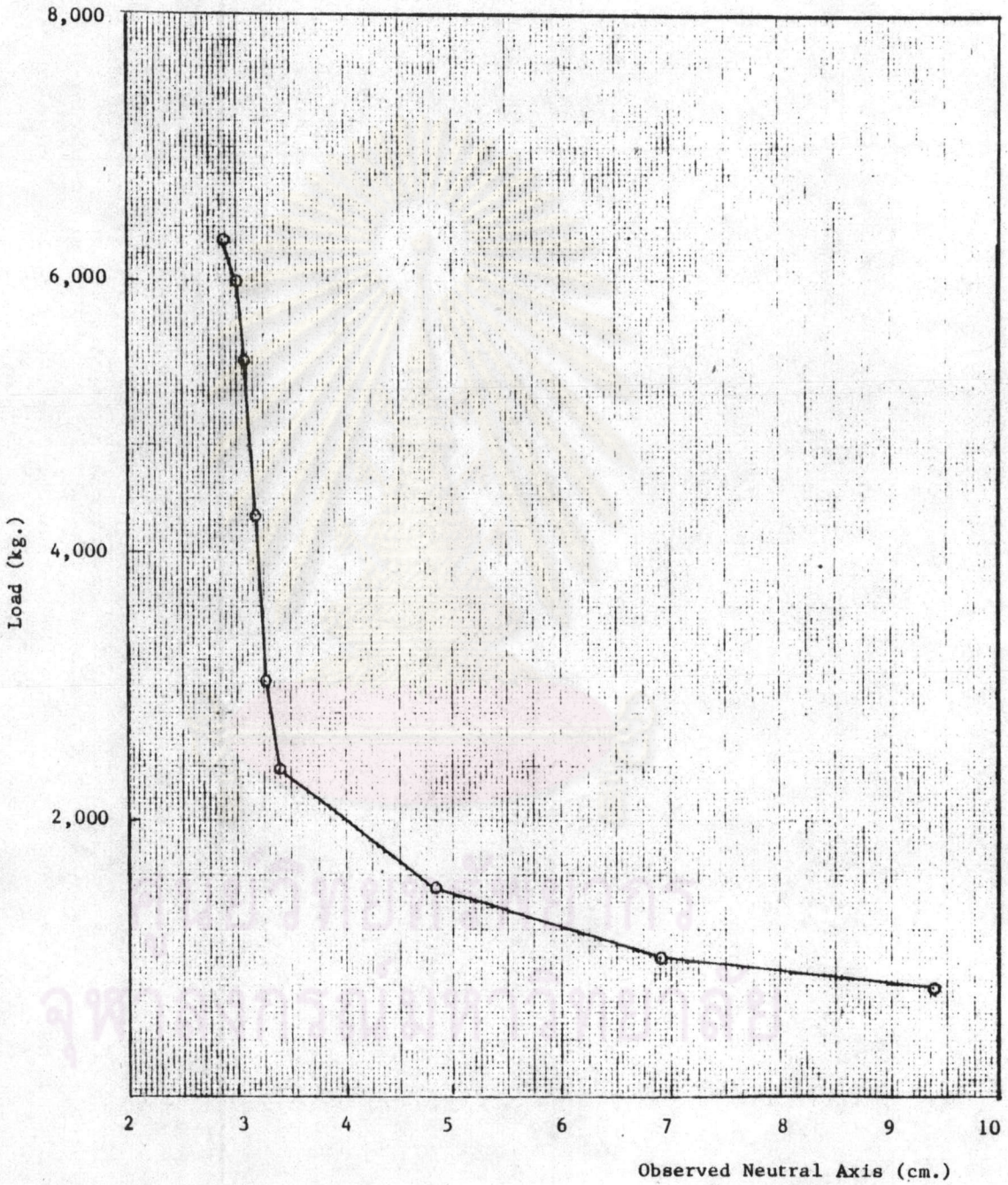

Fig. 4.8 Relationship Between Load and Observed Neutral Axis of B2

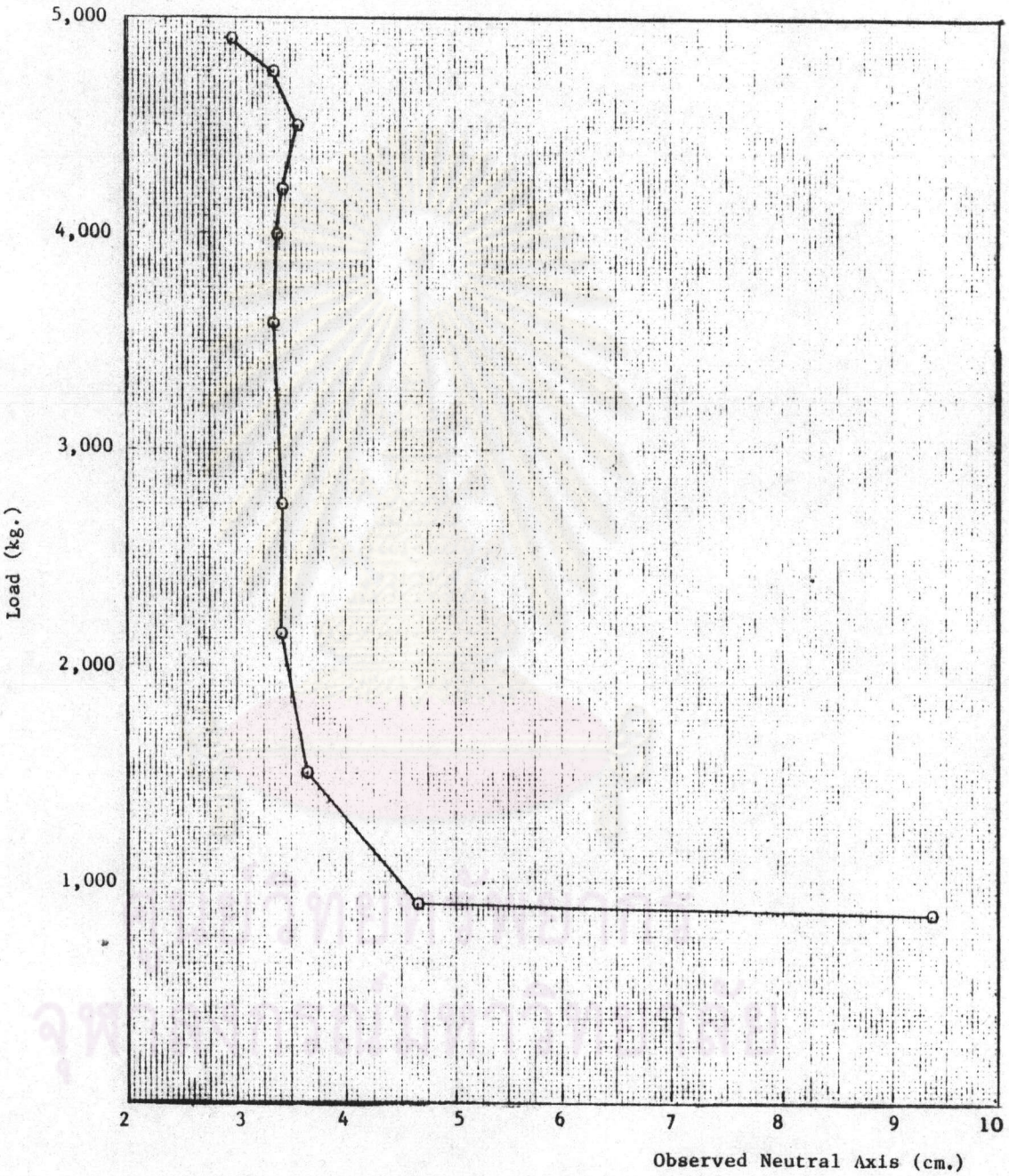

Fig. 4.9 Relationship Between Load and Observed Neutral Axis of B3

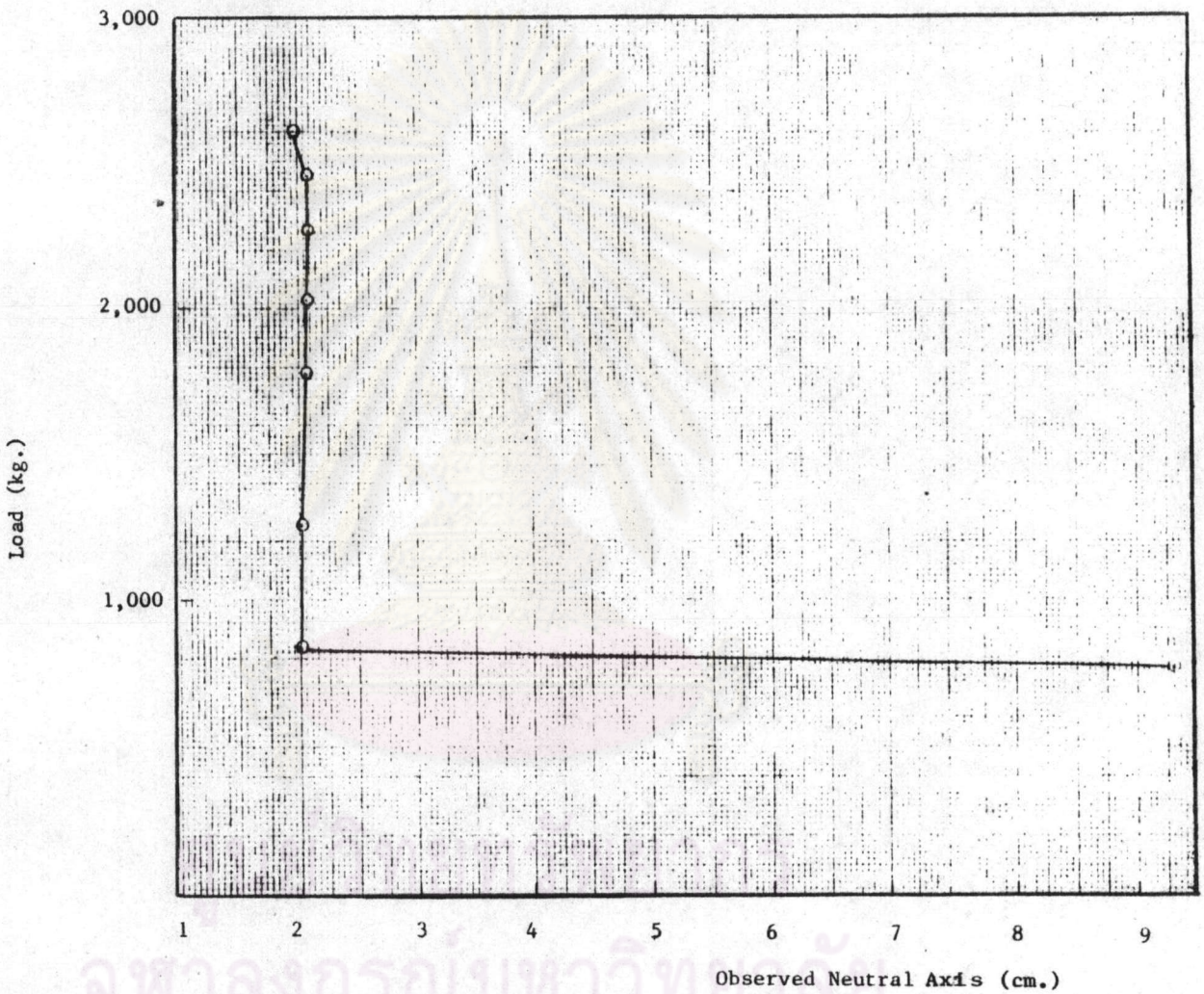

Fig. 4.10 Relationship Between Load and Observed Neutral Axis of B4

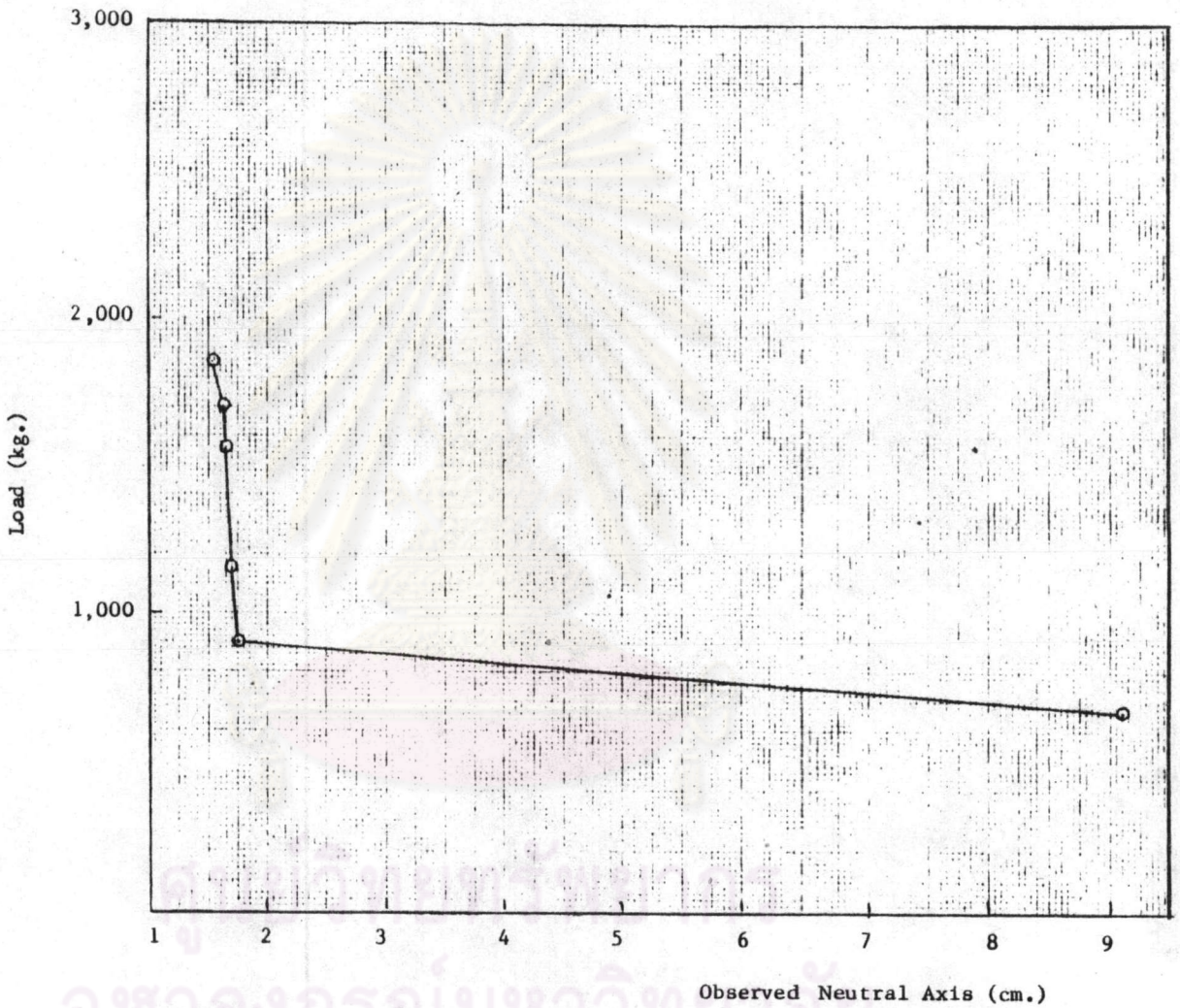

Fig. 4.11 Relationship Between Load and Observed Neutral Axis of B5

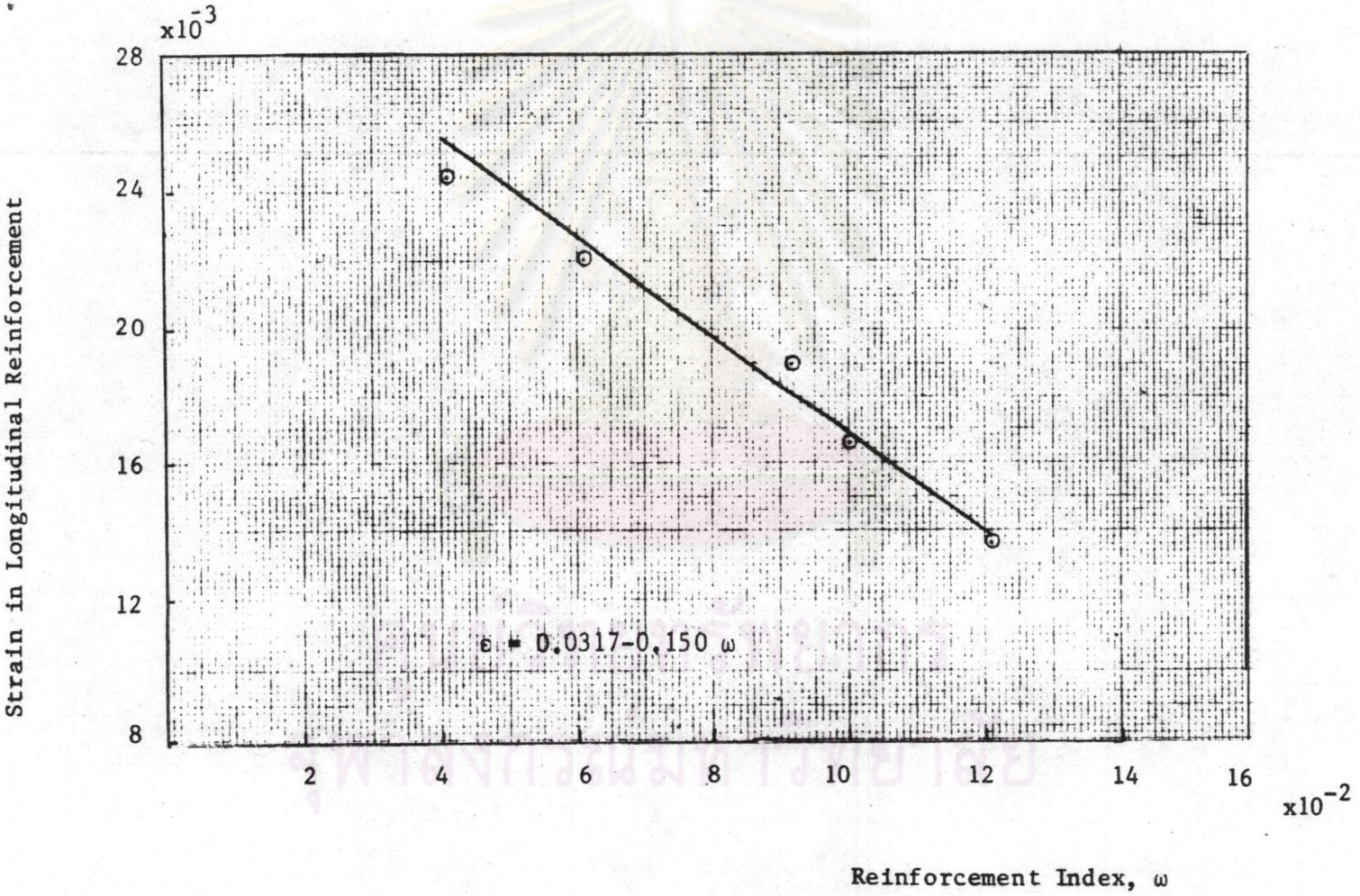

Fig. 4.12 Relationship of Strain in Longitudinal Reinforcement and Reinforcement Index

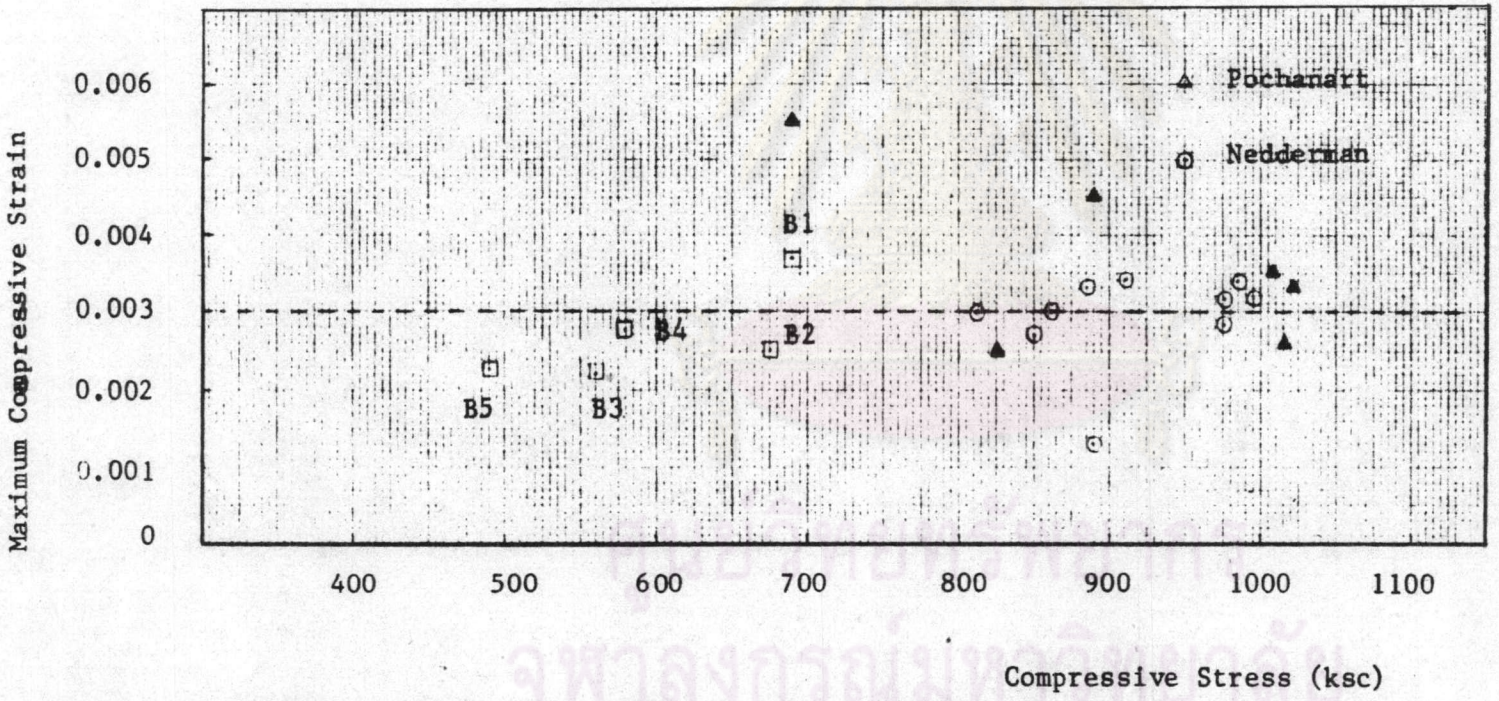

Fig. 4.13 Maximum Compressive Strain and Stress in Test Beams

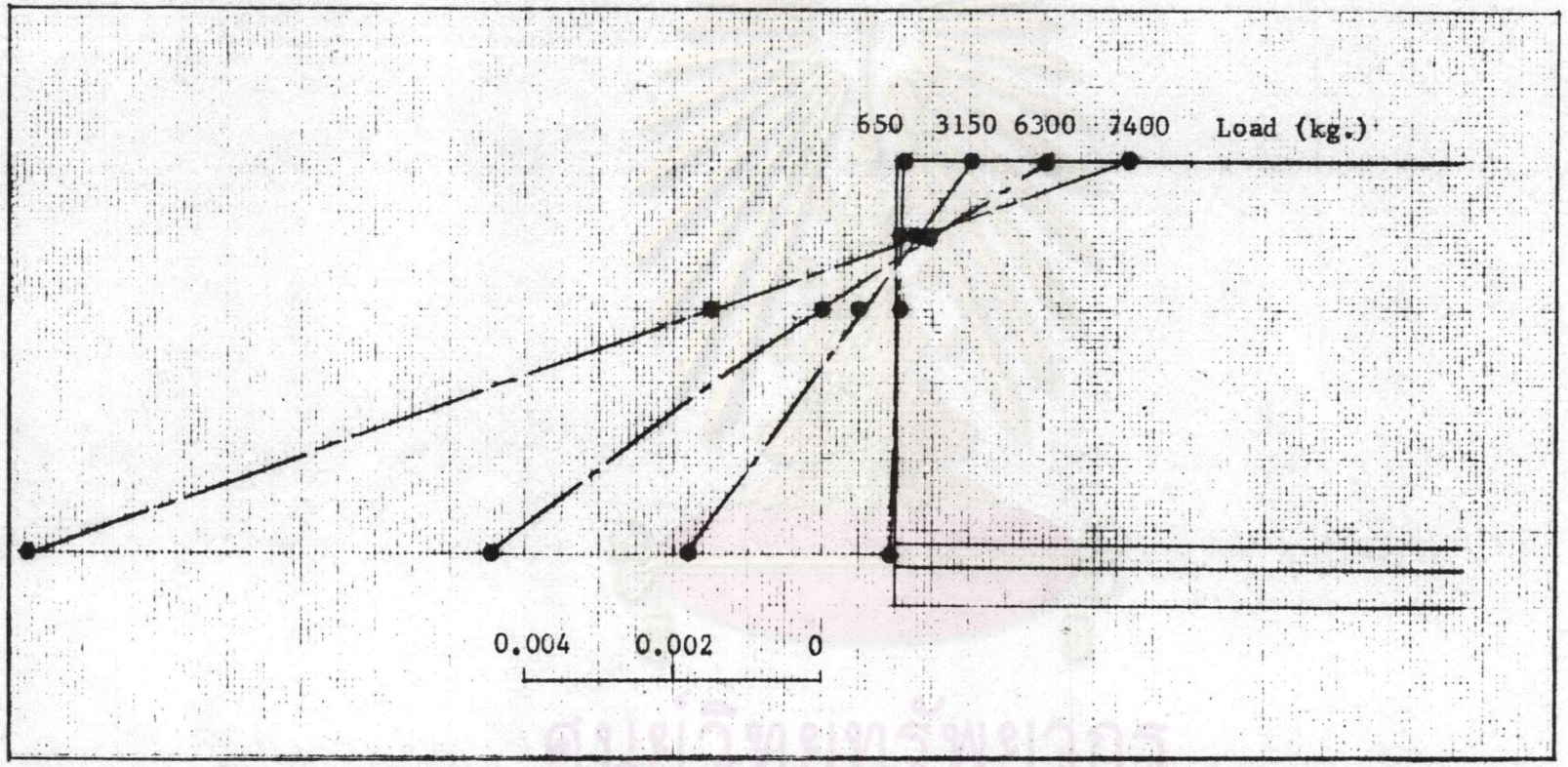

Fig. 4.14 Strain Distribution of B1

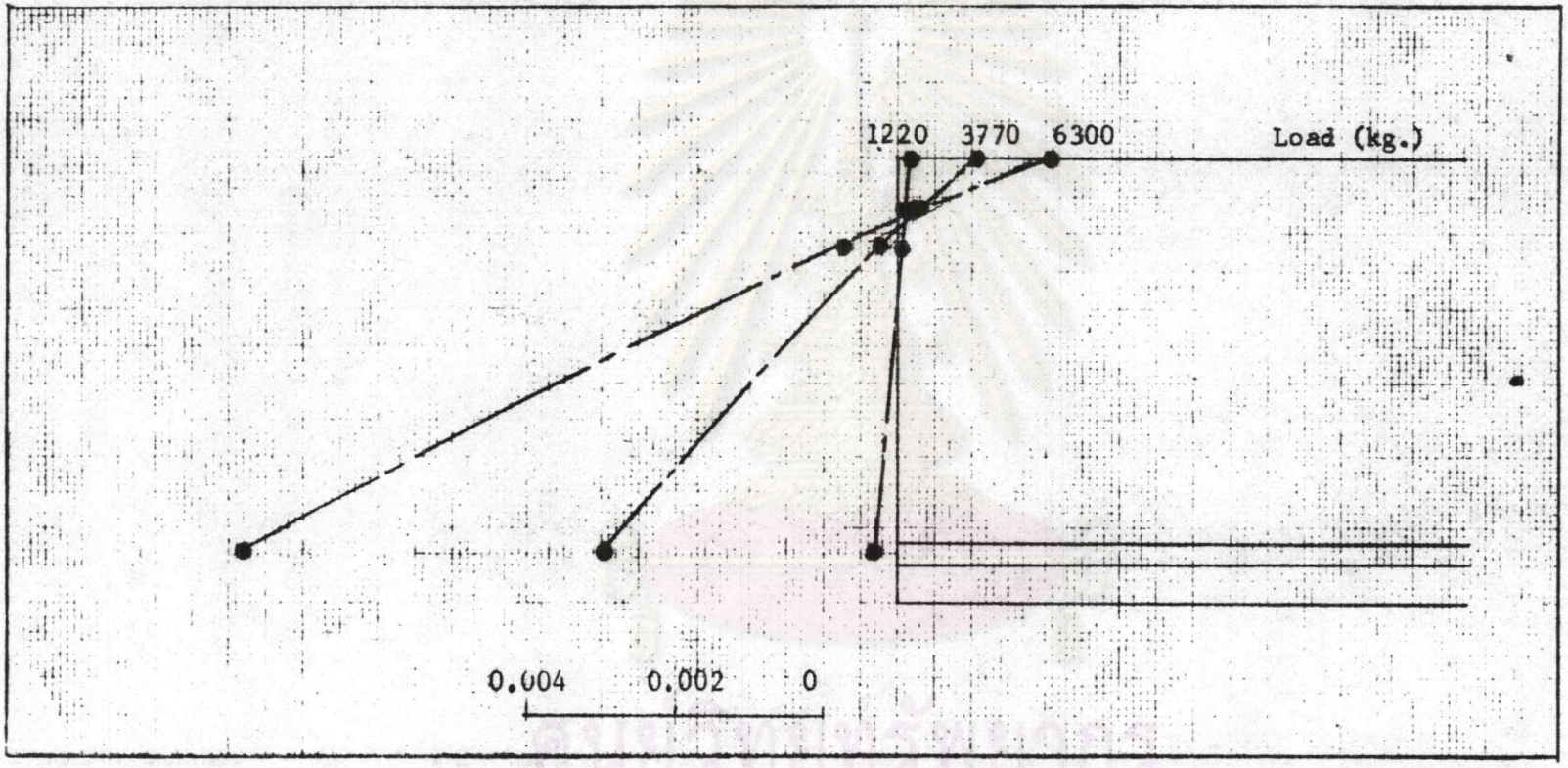

Fig. 4.15 Strain Distribution of B2

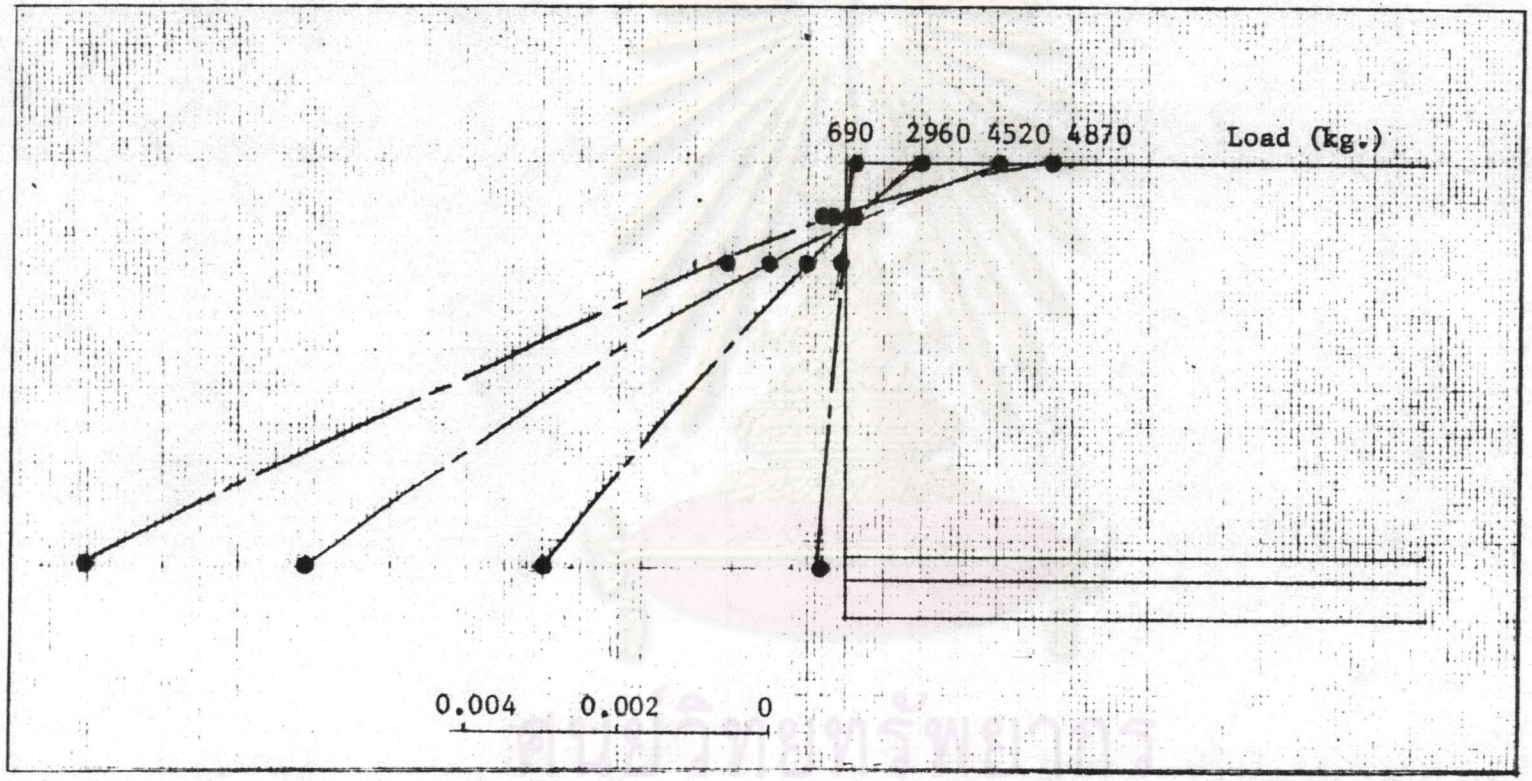

Fig. 4.16 Strain Distribution of B3

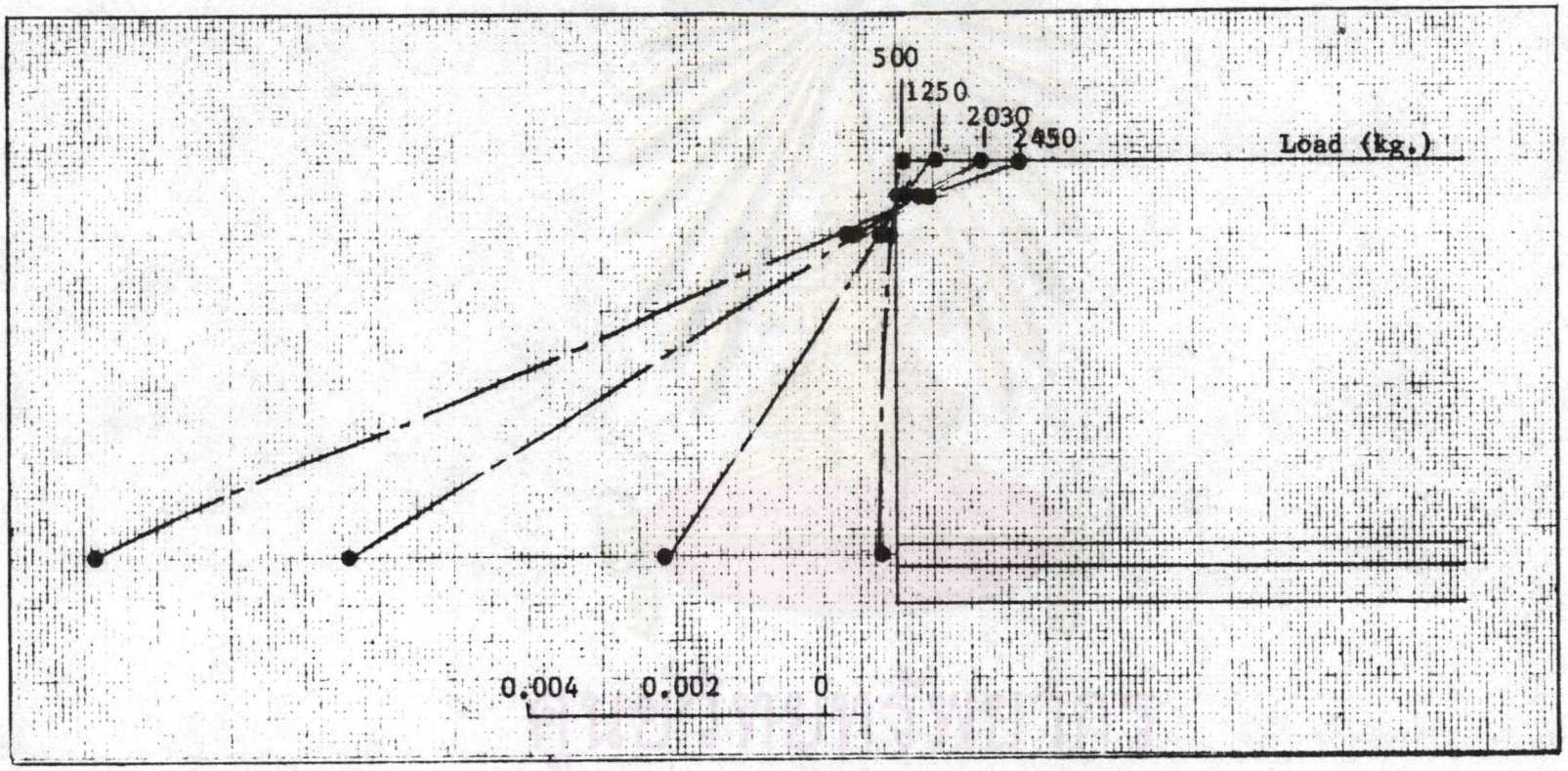

Fig. 4.17 Strain Distribution of B4

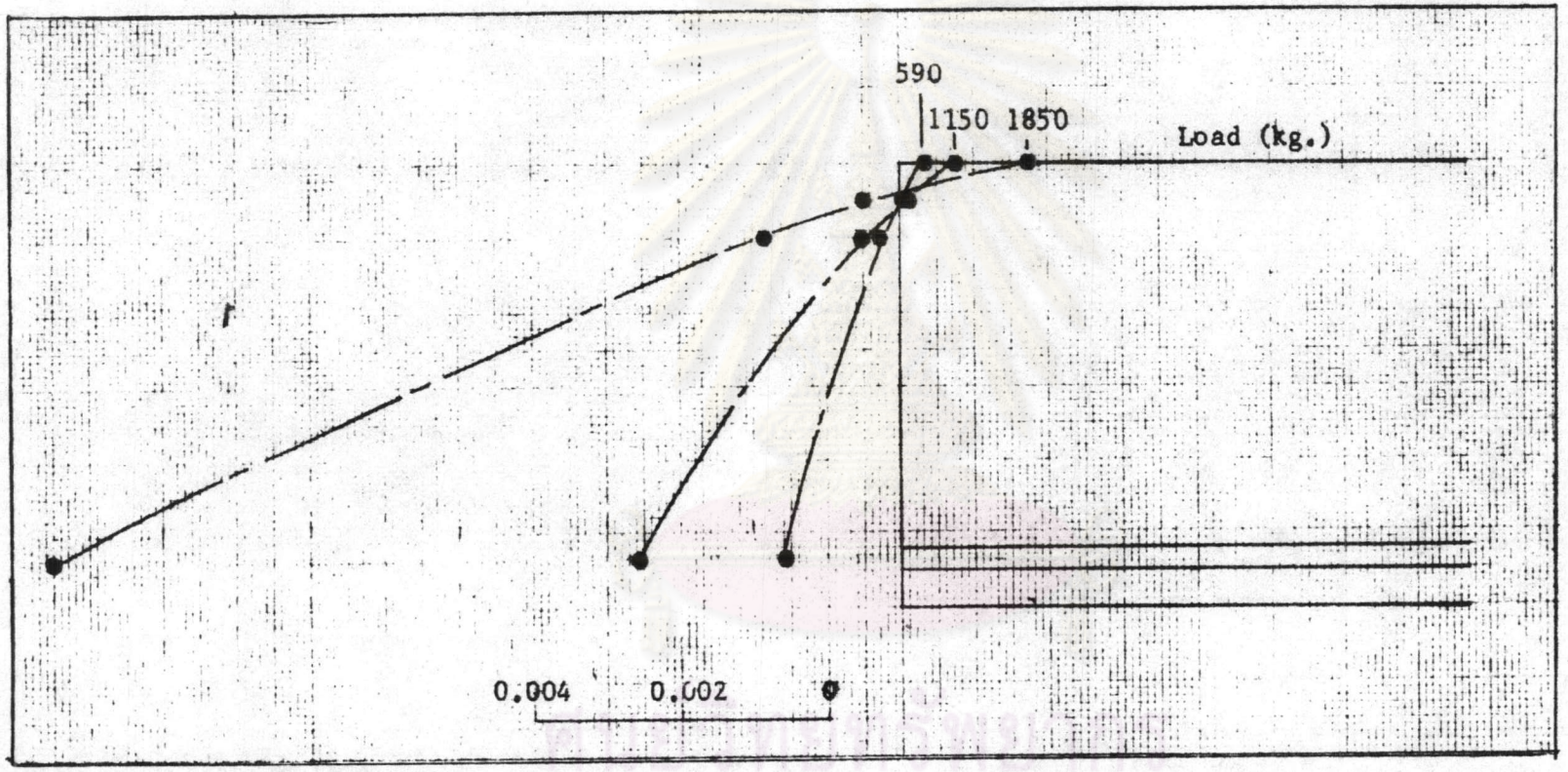

Fig. 4.18 Strain Distribution of B5

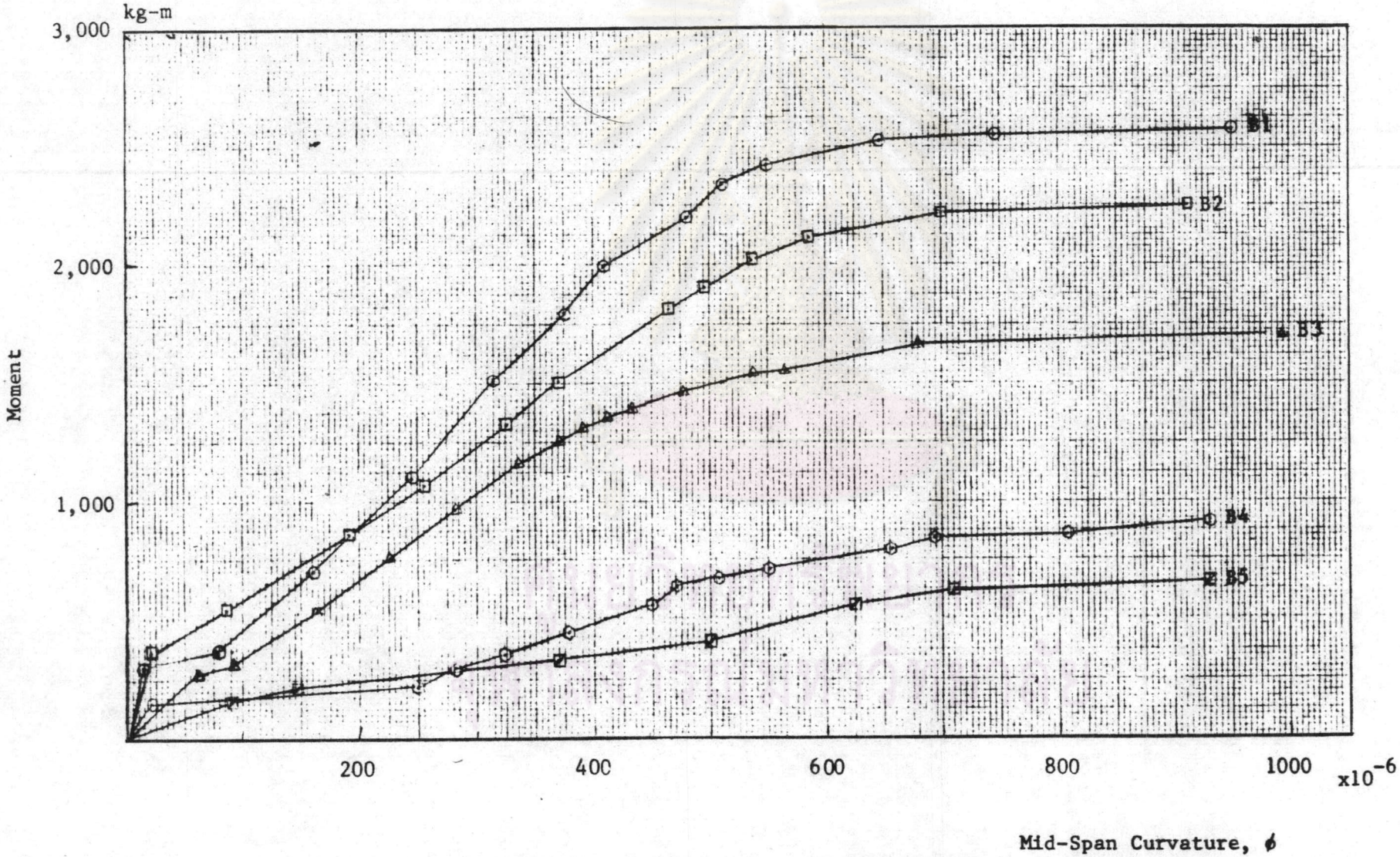

Fig. 4.19 Moment-Curvature Responses of Test Beams

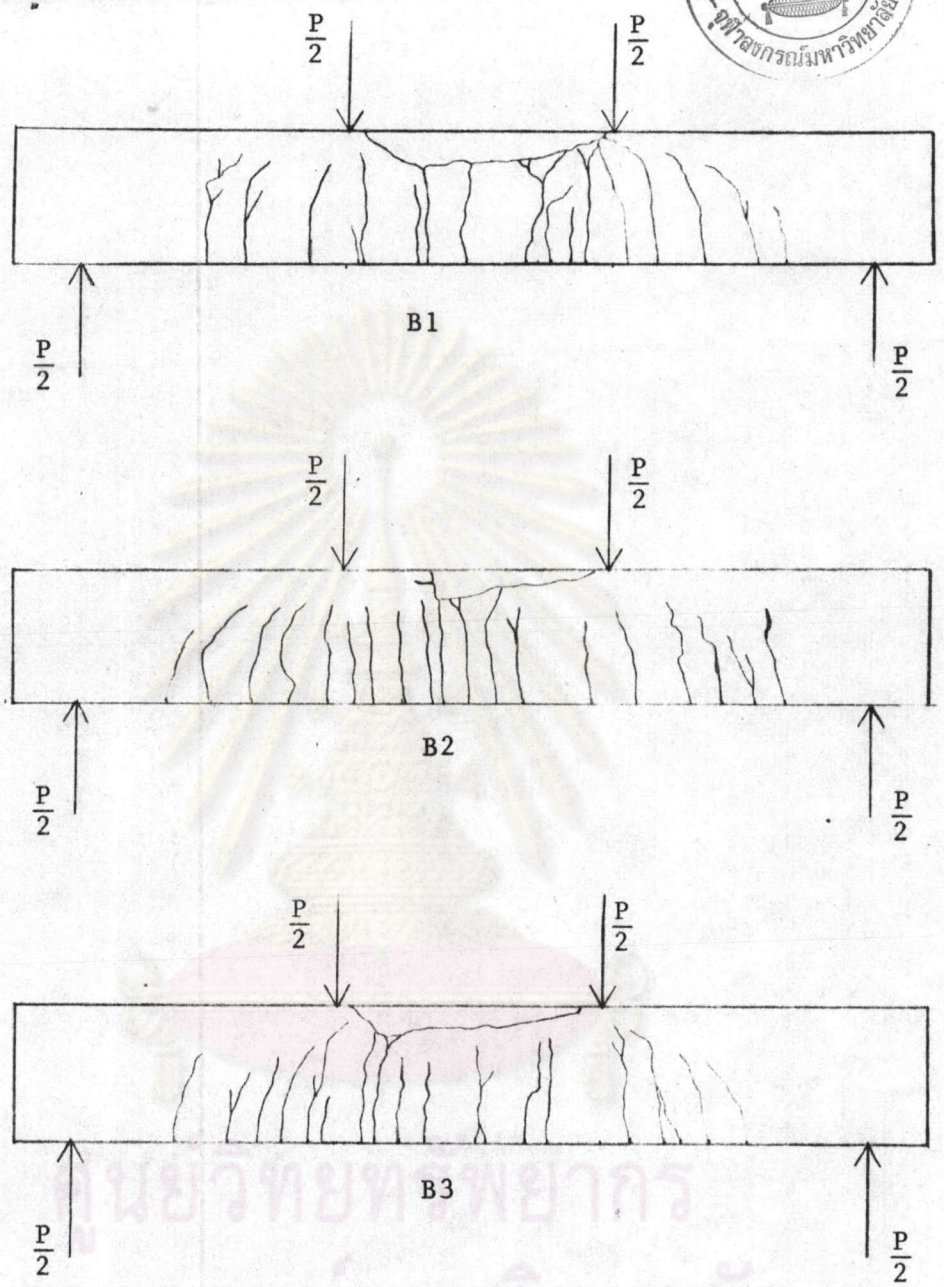

Fig. 4.20 Crack Patterns of B1, B2 and B3

(at 90 percent of ultimate load)

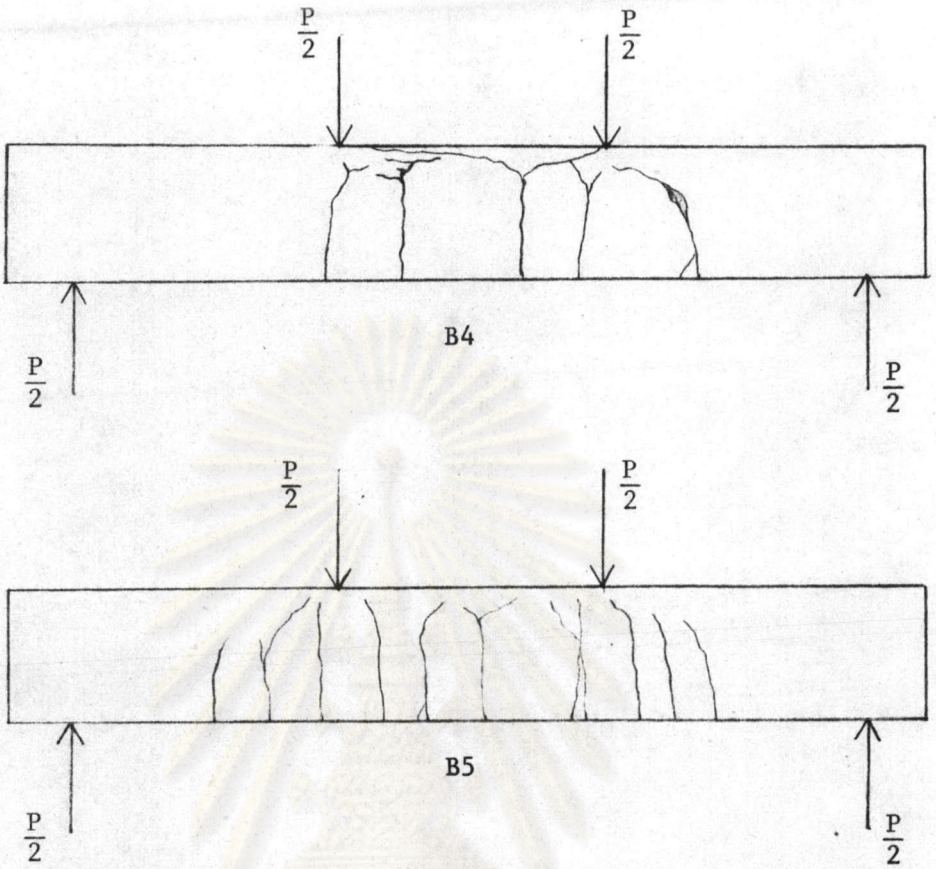

Fig. 4.21 Crack Patterns of B4 and B5

(at 90 percent of ultimate load)

B1

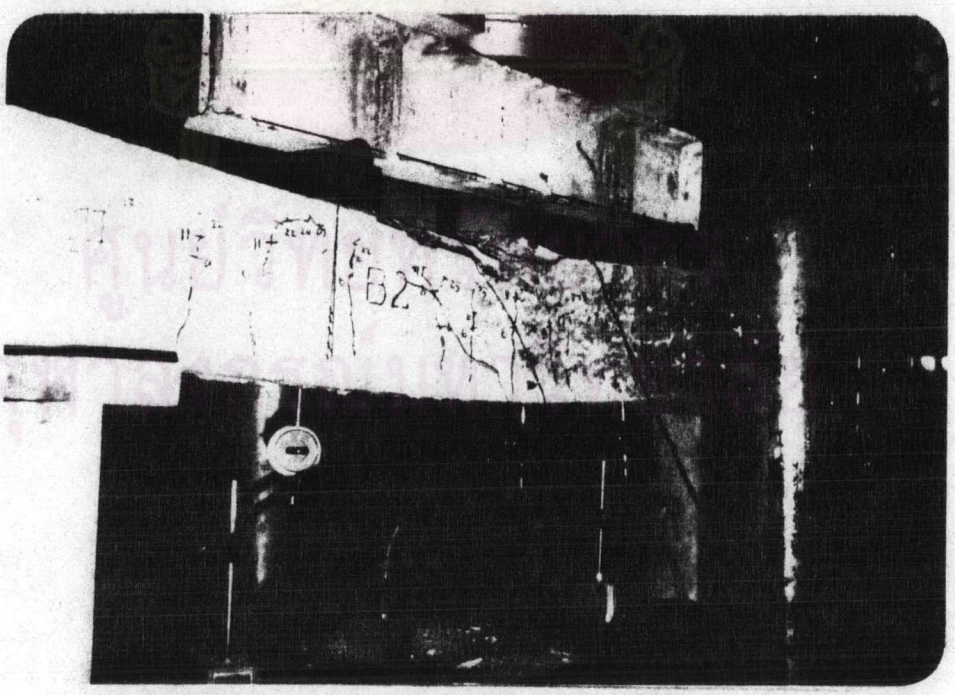

B2

Fig. 4.22 Failure of B1 and B2

B3

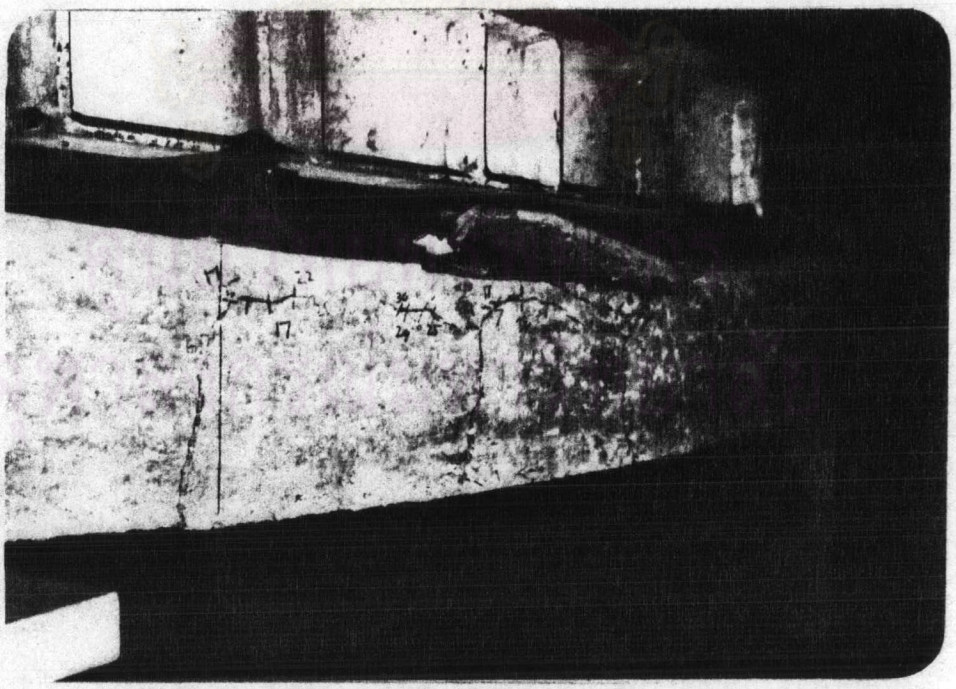

B4

Fig. 4.23 Failure of B3 and B4

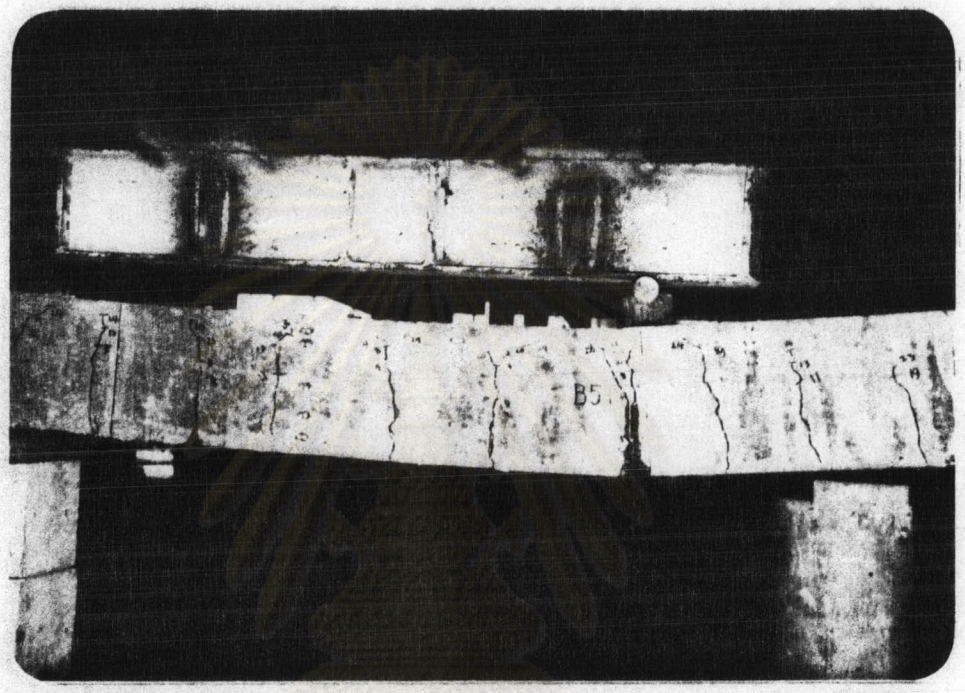

Fig. 4.24 Failure of B5

Table 4.1 Ratio of Load at Controlled Deflection to Ultimate Load of Test Beams

Beam	Reinforcement Index, ω	Loaded at Controlled Deflection $\ell/180$, P_c, kg.	Ultimate Load, P_u	Ratio of P_c/P_u %
B1	0.121	2920	7590	38
B2	0.104	3080	6750	46
B3	0.092	2400	5300	45
B4	0.061	1200	2890	42
B5	0.041	1000	2000	50
			av.	44 %

Table 4.2 Comparison of Observed and Computed Maximum Bending Moments

Beam	M^o_{cr} kg-m	M^c_{cr} kg-m	M^o_u kg-m	M^{1*}_u kg-m	M^1_u/M^o_u	$M^{2!}_u$ kg-m	M^2_u/M^o_u	M^{3+}_u kg-m	M^3_u/M^o_u
B1	290	304	2520	2317	0.919	2308	0.916	2099	0.833
B2	336	302	2100	2016	0.960	2010	0.957	1824	0.868
B3	290	285	1680	1663	0.990	1658	0.987	1504	0.895
B4	210	273	840	1024	1.219	1022	1.216	925	1.101
B5	206	233	590	671	1.137	670	1.135	604	1.024
				av. =	1.045	av. =	1.042	av. =	0.944
				S.D. =	11.390%	S.D. =	11.406%	S.D. =	10.154

* M^1_u is computed by using compressive stress distribution proposed by Nedderman

! M^2_u is computed by using triangular compressive stress distribution

\+ M^3_u is computed by using 1977 ACE equivalent rectangular stress distribution